Available online at www.sciencedirect.com
SCIENCE DIRECT
Journal of Catalysis 228 (2004) 447–459
JOURNAL OF CATALYSIS
www.elsevier.com/locate/jcat

Cetane improvement of diesel with a novel bimetallic catalyst

Mélanie Jacquin [a], Deborah J. Jones [a,*], Jacques Rozière [a], Antonio Jiménez López [b], Enrique Rodríguez-Castellón [b], José Manuel Trejo Menayo [c], Maurizio Lenarda [d], Loretta Storaro [d], Angelo Vaccari [e], Simone Albertazzi [e]

[a] *Laboratoire des Agrégats Moléculaires et Matériaux Inorganiques UMR CNRS 5072, Université Montpellier II, 2, Place Eugène Bataillon, 34095 Montpellier cedex 5, France*
[b] *Departamento de Química Inorgánica, Cristalografía y Mineralogía, Universidad de Málaga, 29071 Málaga, Spain*
[c] *Repsol YPF, S.A. Castellana, 280, 28046 Madrid, Spain*
[d] *Dipartimento di Chimica, Università di Venezia, INSTM UdR di Venezia, Via Torino 155/B, 30173 Mestre VE, Italy*
[e] *Dipartimento di Chimica Industriale e dei Materiali, Università degli Studi di Bologna, INSTM UdR di Bologna, Viale del Risorgimento 4, 40136 Bologna, Italy*

Received 26 April 2004; revised 2 September 2004; accepted 16 September 2004

Available online 5 November 2004

Abstract

Bimetallic Pd–Pt (Pd/Pt mol ratio = 4/1) catalysts supported on a mesoporous aluminosilicate (Si/Al mol ratio = 20) were prepared by direct liquid crystal templating and using three different means of metals incorporation (direct incorporation in the synthesis gel, impregnation, and ion exchange). The method of incorporation affects the accessibility of the metal surface: with impregnation and ion exchange, intermetallic Pd–Pt particles of uniform size are formed, compared to the particles of segregated metal and alloy of different sizes obtained by direct incorporation. Catalysts are characterized by adsorption of nitrogen and hydrogen, and using X-ray photoelectron and extended X-ray absorption fine structure spectroscopies. The activity of the impregnated PdPt catalyst was investigated in naphthalene hydrogenation at atmospheric pressure and at 6.0 MPa in the temperature range from 260 to 340 °C. Using a real diesel feedstock in an industrial microplant, the activity of the PdPt catalyst is higher than that of a state-of-the-art reference, giving 90.0% of aromatics saturation and an 8 points cetane index increase at 280–300 °C. Nonselective cracking products are C_7–C_{10} naphthenes, and, at 325 °C, represent less than 10% product volume. Sulfur poisoning restricts catalyst reactivity mainly to saturation of aromatic molecules, with only limited ring-opening activity, but the final product has a density of 0.840 g cm^{-3} and a maximum distillation temperature (T95 max) of 354 °C and contains less than 3% of polyaromatics, in respect of future European legislation on road diesel.

Keywords: Supported bimetallic catalyst; Hydrogenation/hydrodecyclization; Diesel; Cetane index; Light cycle oil

1. Introduction

The combustion of polyaromatic hydrocarbons contained in diesel produces undesirable emissions. The importance of decreasing the impact of diesel use on air quality has led to increasingly stringent regulations aiming to reduce emissions of particulates, nitrogen, and sulfur oxides by raising the diesel cetane index and lowering the heteroatom content to an acceptable level. In consequence the improvement of middle distillate fuels by conversion of aromatics into hydrocarbons of higher cetane number is today one of the main objectives of the refining industry.

Current technologies for diesel improvement are based on catalysts for hydrogenation and ring opening. Different single-stage or two-stage deep hydrogenation processes have been proposed, but are limited by the conditions used for desulfurization. The single-stage process using conventional catalysts (CoMo, NiMo, NiW on Al_2O_3) is limited by thermodynamic equilibrium conditions at high temperatures. In

* Corresponding author. Fax: +33-4-67 14 33 04.
E-mail address: debtoja@univ-montp2.fr (D.J. Jones).

0021-9517/$ – see front matter
doi:10.1016/j.jcat.2004.09.017

the two-stage process, the use of noble metal catalysts allows hydrogenation at lower temperatures and avoids thermodynamic limitations. However noble metal catalysts are easily poisoned by sulfur or nitrogen present in industrial feedstocks [1,2], and a first step reduction of feedstock sulfur content to a few ppm is necessary before hydrogenation. Numerous two-stage hydrogenation processes have been developed [3–13]. The nature of the catalyst support and the presence of a second metal can also increase the sulfur resistance and current processes use bifunctional-type catalysts, combining acidity of the support for cracking activity, and noble metal hydrogenation properties. Bimetallic sulfur-tolerant Pd–Pt catalysts on various acidic supports including zeolite Y [14–16], zeolite beta [17], gamma zirconium phosphate—silica [18], and gamma alumina [19] have been reported and, in particular, zeolite-supported Pd/Pt-type materials have been considered as the most important industrial catalysts for aromatic hydrogenation [3,6,9,20]. However, the high acidity of a zeolite-type support increases undesirable cracking activity, which accelerates the rate of coke deposition, and other research has focused on the modification of the catalyst acidity and on the use of supports like amorphous SiO_2/Al_2O_3 [17,21–23] or Al_2O_3/B_2O_3 [24–26]. The pore size and topology of the catalyst can influence the activity and selectivity in ring-opening reactions by limiting diffusion of the aromatic components of diesel oil and MCM-41-type mesoporous oxide-supported noble metals have been investigated in the hydrogenation of probe molecules for cracking and hydrotreating light cycle oil [27–29] and in the cetane index improvement of diesel [28,30,31]. The advantage of mesoporosity for accessibility and lower diffusional restriction is also shown by the properties of delaminated ITQ-2 zeolite-supported Pt in aromatic reduction of hydrotreated LCO feed [32].

In this paper we describe the preparation of new bimetallic PdPt catalysts and assessment of their sulfur tolerance and activity in the conversion of “model feedstocks” to hydrogenated and ring-opened products, before evaluation in the improvement of diesel quality using an industrial hydrotreated feedstock. The objective in the preparation of these materials destined to be used in an industrial process is a high conversion, selectivity for hydrogenation and ring opening, and stability in the presence of sulfur. The support, in particular its pore structure and acidity, and the catalyst metal dispersion are important factors affecting the catalytic behavior.

The support used for these catalysts is a mesoporous aluminosilicate matrix obtained using a nonionic surfactant and with the direct liquid crystal templating (DLCT) method we have developed and reported [33]. This method, leading to a material with surface acidity (number and strength of the sites) lower than that of zeolites [34,35] and with pore dimension tailored by the nature of the nonionic surfactant, has been previously employed for the synthesis of rhodium-, platinum-, iridium-, or ruthenium-containing catalysts for the hydrogenation and ring opening of naphthalene [36].

Several different means for metal incorporation in porous supports are described in the literature [37] and we concentrate here on three. The first method is by direct coincorporation of palladium and platinum propanedionates into the synthesis gel followed by thermal treatment to remove surfactant porogen and reduction under hydrogen, the method employed for the analogous monometallic (Rh, Pt, Ru, and Ir) catalysts [36] or Rh-functionalized MCM-41 [38,39]. In this way, depending on its nature, the metal is introduced into the silico-aluminate structure and/or the pores [40,41]. The second method is the impregnation of the calcined support by a solution of palladium and platinum salts followed by thermal treatment. The last route is the neutralization of the surface Brønsted acidity with ammonia followed by ion exchange with appropriate complexed metal ions. These methods lead to three types of Pd/Pt-supported aluminosilicate. Catalytic activity and thiotolerance depend on the Pd/Pt ratio, and molar ratios in the range 4/1–6/1 have been reported as the most appropriate [15,21].

We describe below the preparation and physical–chemical characterization of the three Pd/Pt-supported aluminosilicates and the behavior of the impregnated catalyst toward naphthalene hydrogenation at 200–340 °C, in preliminary work under atmospheric pressure and then at 6.0 MPa, and in the presence of a sulfur-containing poison. The performance of this catalyst in aromatic saturation and cetane index improvement of a hydrogenated light cycle oil feedstock containing 50 wt ppm sulfur are reported, as well as the composition of the light (< 180 °C) fraction, of importance in the context of process design.

2. Experimental

2.1. Catalyst preparation

The aluminosilicate support of the bimetallic catalysts was synthesized using a Brij 30 (C_{12}–$C_{25}(EO)_4$) surfactant and with a Si/Al ratio of 20. All materials contained 2.0 wt% of the two metals, and a Pd/Pt molar ratio of 4/1.

A first catalyst was synthesized by direct incorporation of Pd/Pt into the synthesis gel. The preparation was carried out at 65 °C. Brij 30 (4.5 g, Aldrich) was dispersed in aqueous HNO_3 solution (4.5 g, 0.1 mol dm^{-3}; 65% nitric acid solution from Aldrich). To this solution were added tetraethoxysilane (TEOS, Fluka, 13.0 g) and aluminium nitrate ($Al(NO_3)_3 \cdot 9H_2O$, Merck, 1.2 g). $Pd(CH_3COCHCOCH_3)_2$ (0.076 g) and $Pt(CH_3COCHCOCH_3)_2$ (0.025 g) were then incorporated successively, and the mixture was stirred until all reagents were dissolved. The solution was transferred to a crystallizing dish in a desiccator and the latter held under dynamic vacuum for 2 h, and then left at room temperature for 72 h. The surfactant was then removed from the solidified gel by calcination at 560 °C for 4 h using a ramp rate of 1 °C/min. This catalyst is denoted PdPt-Dir in the following.

A second catalyst was prepared by impregnation of a Pd/Pt solution into a calcined silicoaluminate support prepared as above, but without addition of palladium and platinum organics. One gram of the support was first sieved to 0.8–1 mm and dried at 100 °C for 12 h before incipient wetness impregnation with $PtCl_4$ and $PdCl_2$ to give 2.0 wt% metals in the final catalyst. The impregnated solid was calcined at 120 °C for 2 h and 560 °C for 2 h with a 2 °C/min ramp. This catalyst is denoted PdPt-Imp.

A third catalyst was prepared by ion exchange. The support was prepared and sieved as described above. After drying at 100 °C for 12 h, it was left in a closed vessel containing ammonia vapor. The ammonium-ion-functionalized material was then contacted 12 h with 100 cm^3 of an aqueous solution of 0.011 g of $(Pt(NH_3)_4Cl_2 \cdot H_2O)$ and 0.034 g of $(Pd(NH_3)_4Cl_2 \cdot H_2O)$ (Pd/Pt in ratio 4/1) in an amount allowing a total metal loading of 2.0 wt%. The material was then recovered by filtration, washed, dried, and calcined 4 h at 560 °C with a 2 °C/min ramp. This catalyst is denoted PdPt-IE.

2.2. Catalyst characterization

To determine the specific surface area and the porosity of the materials, adsorption–desorption of nitrogen at −196 °C was performed using an automated volumetric instrument developed in-house. Samples were outgassed overnight at 200 °C under vacuum prior to the experiments. The surface area was determined using the BET formalism [42] and the pore diameter was estimated using the α_s method. Determination of surface acidity was based on ammonia chemisorption. The amount of NH_3 adsorbed at different partial pressures in the equilibrium bulk phase was measured using a Micromeritics ASAP 2010C apparatus. Prior to adsorption measurements, the solid sample was outgassed at 350 °C for 3 h. Thereafter, to reduce physisorption of ammonia on the solid surface, the adsorption temperature was evacuated at 80 °C. Successive ammonia doses were flushed onto the sample until a final equilibrium pressure of 5 kPa was reached. The equilibrium pressure was measured after every adsorption step, and the amount adsorbed was calculated. At the end of the first adsorption cycle, the sample was pumped at 80 °C for 30 min, and a second adsorption cycle was then performed at the same temperature. The difference in adsorption between two adsorption cycles is ascribed to irreversible adsorption of NH_3. This quantity first changes as the adsorption progresses, but then levels off. The irreversible adsorption of NH_3 corresponds to the localized chemisorption of NH_3 molecules and it provides the total number of surface acid sites.

TEM observations were made on samples prepared as extractive replicas using a JEOL 1200 EX operating at 100 kV. The accessible metal surface was measured by H_2 chemisorption using the Micromeritics ASAP 2010C. Samples were first flushed in a flow of He, and then evacuated before chemisorption with H_2 at 300 °C. The metal particle size was estimated from the relation: $D\% = 1000/d$ with $D\%$ = metal dispersion and d = metal particle diameter in Å.

XPS analyses were performed using a Physical Electronic 5700 instrument with Mg-$K\alpha$ and Al-$K\alpha$ radiation ($h\nu = 1253.6$ and 1486.6 eV, respectively), using a hemispheric electron analyzer. The catalyst precursors (supported metal oxide) and catalysts (after reduction) were studied in order to follow the evolution of the metal environment in samples in which the metal had been incorporated in different ways. Binding energies (BEs) were determined with an accuracy of ±0.1 eV. Charge referencing was measured against adventitious carbon (C 1s 284.8 eV). The residual pressure in the analysis chamber was maintained below 10^{-7} Pa during all measurements.

EXAFS spectra were measured on the EXAFS13 spectrometer, line D42, at the LURE synchrotron (Laboratoire pour l'Utilisation du Rayonnement Electromagnétique, Paris), at the Pt L_{III} (11,564 eV) and Pd K (24,350 eV) edges. Energy calibration was carried out using corresponding metal foils of 10 and 25 μm thickness and with E_0 defined as the first inflection point in the rising edge. EXAFS spectra were recorded in transmission mode to 1000 eV after the absorption edge with a 3 eV step between each point of measurement. I_0 and I_1 ion chambers were filled respectively with air/argon for experiments at the Pt L_3 edge and with krypton for those at the Pd K edge. Experimental data were analyzed using computer codes developed by Michalowicz [43]. The analysis process included: (i) extraction of the EXAFS signal $\chi(k)$ from the absorption spectrum $\mu(E)$ using $\chi(k) = (\mu - \mu_1)/(\mu_1 - \mu_0)$, where μ_0 was obtained by linear fitting of the continuous background before the absorption edge, and the low-frequency term, μ_1, corresponding to the slow decay beyond the edge was modeled by a third order polynomial. The edge threshold energy E_0 was selected as the first point of inflection of the edge; (ii) calculation of the EXAFS Fourier transform (FT) radial distribution-like function $F(R)$ over the range 3–15 $Å^{-1}$, and k^3 weighting; (iii) filtering of the successive coordination spheres in $F(R)$ and calculation of their inverse Fourier transform to obtain partial components of the EXAFS spectra; (iv) multivariate least-squares fitting of the filtered EXAFS spectra using photoelectron phase and amplitude functions derived using Feff [44], a variable photoelectron mean free path, fixed-scale factor S_0^2 equal to 0.8 and energy shifts (determined from partial components simulation for each sample). In this way, the number of nearest neighbors, N_i, the interatomic absorber-neighbor distance, R_i, and the Debye–Waller-type factor, σ_i, were obtained for each coordination shell of atoms.

2.3. Catalyst activity

The catalytic activity of PdPt-Imp in the hydrogenation of naphthalene was first investigated in a fixed-bed lab-scale microreactor, operating at atmospheric pressure, at 200 and

300 °C. The bed, containing 200 mg of the H_2/N_2-reduced catalyst, was in contact with a continuous flow of naphthalene/He (0.1 g/10 cm^3). The reaction products were analyzed by gas chromatography. The thiotolerance of the catalyst was examined at 200 °C and atmospheric pressure, using benzo(*b*)thiophene as sulfur-containing poison. In this system, the H_2 flow (300 cm^3/min) passed through the naphthalene-containing saturator and after every gas-sample valve injection, the hydrogen flow was switched through the benzo(*b*)thiophene-containing saturator for 10 s. The flow was then switched back to naphthalene for 15 min. The weight hour space velocity was 0.2 h^{-1}. The pulses were started after reaching a constant activity in naphthalene hydrogenation (2 h of reaction with a sulfur-free feed). The number of pulses that caused a 25% decrease of the conversion was used as criterion to compare the thiotolerance of the catalysts.

Following this preliminary evaluation, the catalytic activity was fully investigated at 6.0 MPa using PdPt-Imp using the experimental setup described previously [36]. Employing a contact time and H_2/organic feed ratio fixed at 6.8 s and 21 mol/mol, respectively, the influence of reaction temperature on naphthalene conversion was investigated and the activity and selectivity were compared with those of a state of the art reference catalyst [12]. Addition of dibenzothiophene (DBT) in the feed allowed determination of the stability of the catalyst toward sulfur poisoning. DBT is frequently used as source of sulfur in model feedstocks [15,23,45], although hydrogen sulfide and thiophene have also been used [46].

Evaluation of the catalyst capacity to improve cetane index was carried out using a hydrotreated light cycle oil (LCO) feed stream. The evaluation was made by comparison with the above reference catalyst. The feed stream was hydrotreated using a conventional CoMo catalyst at 360 °C, 6.0 MPa, and LHSV = 1 h^{-1} until a sulfur content of $\leqslant$ 50 wt ppm was obtained. Two hydrotreated streams were used (Table 5): HT1 for the reference catalyst and HT3 for PdPt-Imp, the latter was used in the form of sieved monoliths (25 cm^3 of PdPt-Imp sieved in the range 1.5–2.5 mm), and the former as extrudates (size 1.5–2 mm), and both were first diluted with carborundum in a ratio 1:1. They were activated in situ before testing according to the following procedure: drying, 120 °C, 1 h, N_2 flow (600 N cm^3/min); reduction, 400 °C, 2 h, H_2 flow (600 N cm^3/min), 6.0 MPa; stabilization, 285 °C, 12–48 h, feedstock flow (H_2/feed = 600 N cm^3/cm^3, LHSV = 1 h^{-1}). Catalyst testing was performed at temperatures between 270 and 345 °C under constant pressure of 6.0 MPa, with constant H_2/feed ratio and space velocity. The products were identified by HPLC and gas chromatography and the cetane number determined according to ASTM-D-4737.

3. Results and discussion

3.1. Catalyst characterization

All three catalysts showed fully reversible nitrogen adsorption isotherms with a quasilinear region from 0.1 to 0.3 indicative of supermicroporosity. The derived BET surface areas are between 645 $m^2\,g^{-1}$ (ion-exchanged material) and 884 $m^2\,g^{-1}$ (direct incorporation), and the mean pore diameter, 2.2 nm, is around the lower limit of mesoporosity (Table 1). The support silicoaluminate prior to impregnation has a specific surface area of 999 $m^2\,g^{-1}$ and a mean pore diameter of 2.6 nm. The incorporation of metals in the structure therefore leads to a slight decrease in the surface area but the pore diameter and the mesoporous character are maintained. It is also important that the incorporation of noble metals into the support leads to catalysts with appropriate surface acidity. After reduction in H_2, the average number of acid sites of the reduced catalyst is comparable to that of the support (ca. 300 µmol g^{-1}). The higher acidity of the oxide form precatalyst (440 µmol g^{-1}) is due to an increased number of Lewis acid sites, associated with the presence of transition metal oxides.

Fig. 1 shows the hydrogen adsorption isotherms of the three materials. For those prepared by impregnation and ion exchange, a plateau is rapidly reached and thereafter the quantity of adsorbed H_2 slightly increases with pressure. In contrast, for the material prepared by direct incorporation, the isotherm is different since a continuous increase in H_2 absorption is observed, which corresponds to H_2 diffusion into particles of palladium metal [47]. This result might suggest that, in the case of PdPt-Dir, at least part

Table 1
Textural properties, dispersion, and metal particle size of supported PdPt catalysts

	Direct incorporation (Dir)	Impregnation (Imp)	Ion exchange (IE)
Surface area ($m^2\,g^{-1}$)	884	732	645
Pore diameter (nm)	2.2	2.2	2.2
Metal dispersion (%)	7	25	28
Metal surface area ($m^2\,g^{-1}$ catalyst)	0.20	1.88	1.99
Metal surface area ($m^2\,g^{-1}$ metal)	28	94	107
Particle diameter (nm)			
From dispersion	14.4	4.0	3.6
From TEM	2.5 and 4.0–7.0	3.5	3.0

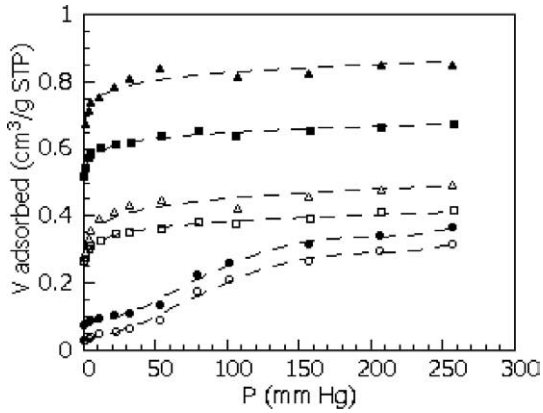

Fig. 1. H_2 chemisorption isotherms of PdPt-Dir (●, ○), PdPt-Imp (■, □), and PdPt-IE (▲, △). Full symbols, first analysis; empty symbols, repeat analysis.

of the palladium is segregated into monometallic particles whereas isotherms of PdPt-Imp and PdPt-IE are compatible with the existence of intermetallic particles, as deduced previously from EXAFS and TEM for other bimetallic Pd–Pt systems [48]. The method of metal incorporation strongly influences the properties of metal dispersion and derived metal particle sizes obtained from H_2 chemisorption and transmission electron microscopy (Table 1). The catalyst prepared by direct synthesis has a dispersion of less than 10% and a large metal particle size, while for that prepared by impregnation, small, well-dispersed particles (4 nm), four times smaller than those in PdPt-Dir are identified. Ion exchange gives the highest dispersion, with metal particle size of 3.6 nm. Junges et al. [49] have observed a similar effect with a palladium on MCM-41 support, when the metal particle size decreased in the order: direct incorporation, impregnation, ion exchange.

These conclusions are supported by observation of the extractive replica TEM images in Fig. 2. For the material prepared by direct synthesis, two types of particle are observed, those of size ca. 2.5 nm that could correspond to a metal alloy, and larger particles of 4.0–7.0 nm probably corresponding to segregated single metal particles. The micrographs of the impregnated and ion-exchanged materials show only one type of particle of size 3.0–4.0 nm. The metal particle diameter of PdPt systems previously described in the literature varies in the range from 2 to 4 nm [48–50], and incorporation by impregnation and ion exchange seems to lead to smallest metal aggregates.

Measurement of the diameter of more than 500 particles in the TEM micrograph of PdPt-Imp provided an indication of the distribution of particle size. The method employed [51] leads to the histograms shown in Fig. 3. The first of these (Fig. 3a) provides a distribution in diameter with a mean diameter of $\sum n_i d_i / \sum n_i$, while the second (Fig. 3b) is a quadratic distribution with a mean diameter of $\sum n_i d_i^3 / \sum n_i d_i^2$ (n_i, number of particles and d_i, mean diameter, in each successive interval). The second distribution is probably the most relevant since catalyst activity is directly linked to the metal surface area developed by the particles. The distribution is narrow, with 45% of the metal particles of size between 2 and 3 nm, with 43% of the metal surface area resulting from particles between 3 and 4 nm in diameter. The mean surface diameter, 3.5 nm, is in good agreement with the value estimated from H_2 chemisorption.

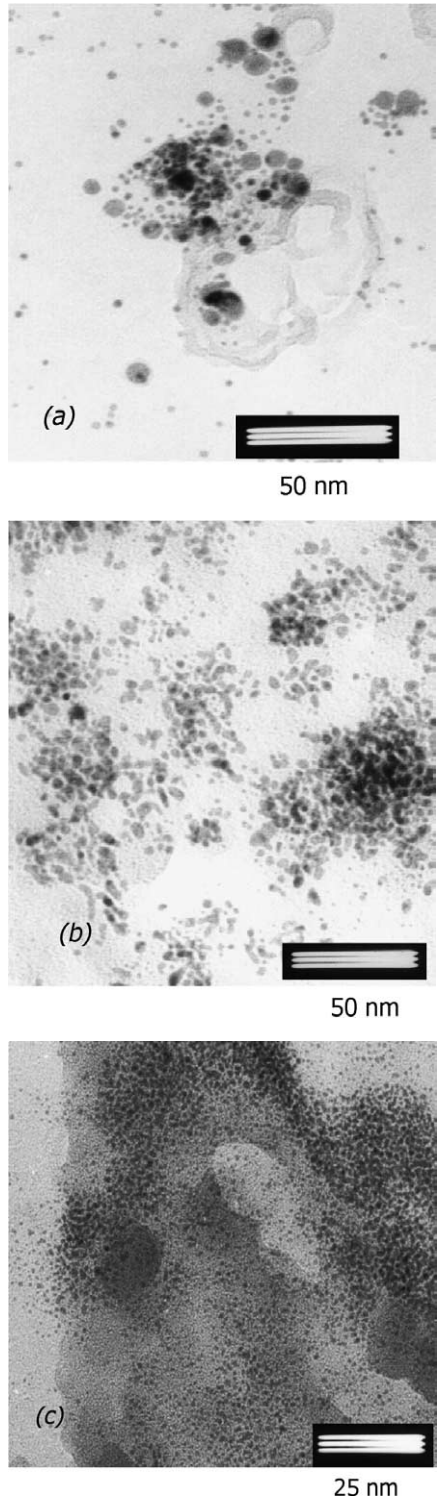

Fig. 2. Transmission electron microscopy images of 2PdPt PdPt-Dir (a), PdPt-Imp (b), and PdPt-IE (c).

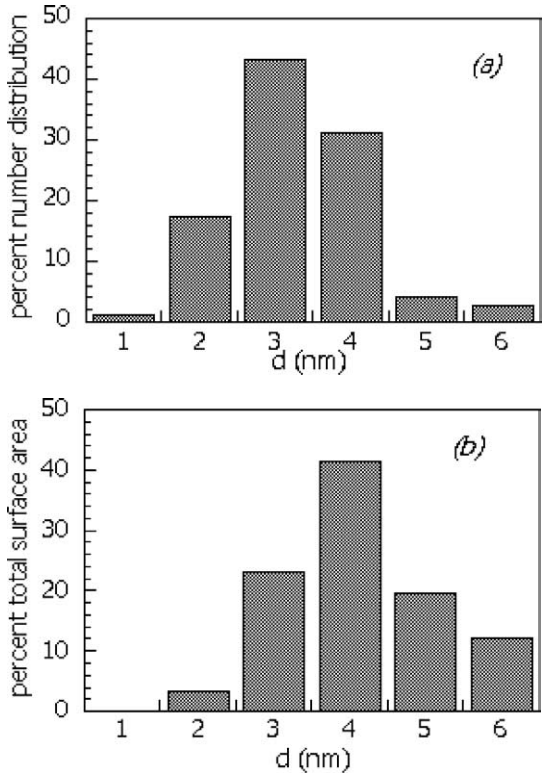

Fig. 3. Mean article diameter of PdPt-Imp obtained from the number (a) and the quadratic (b) distributions.

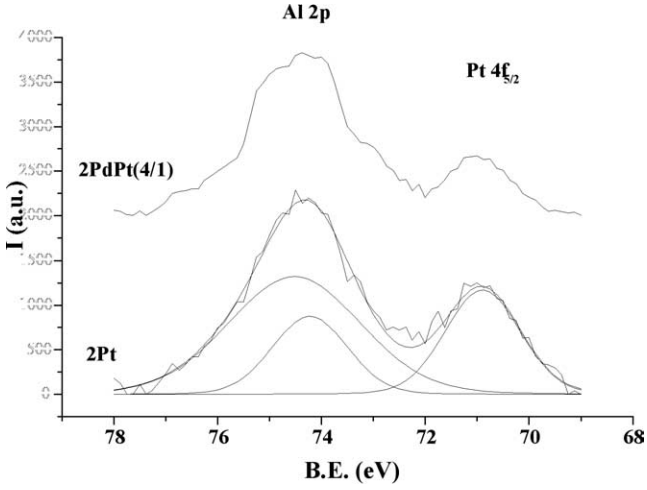

Fig. 4. X-ray photoelectron spectrum of PdPt-Imp and Pt-Imp in the Al 2p and Pt 4f region.

Table 2 lists the positions of XPS signals for the three Pd/Pt catalysts after reduction and the XPS spectra of samples Pt-Imp and PdPt-Imp in the Al 2p and Pt 4f region are shown in Fig. 4. Due to the low concentration of aluminium in the support, the Al 2p signal presents a relatively low intensity signal, and the Pt $4f_{7/2}$ peak is clearly observable at about 71.0 eV, even in the case of a sample with a low Pt content such as sample PdPt-Imp. This binding energy value of 71.0 eV is assigned to the presence of Pt(0). The spectrum of sample Pt-Imp has been deconvoluted into three peaks. Two

Table 2
XPS data for supported Pd/Pt catalysts

Sample	Binding energy (eV)					Surface atomic ratio
	O 1s	Si 2p	Al 2p	Pt $4f_{7/2}$	Pd $3d_{5/2}$	O/(Si + Al)
PdPt-Dir	532.7	103.1	74.4	70.7	334.8	2.15
PdPt-IE	532.6	102.9	74.4	70.8	335.0	2.02
PdPt-Imp	532.8	103.1	74.7	71.0	335.3 (80%)	2.13
					336.8 (20%)	

Table 3
Structural parameters derived from EXAFS analysis at Pd and Pt edges

	r(Pt–Pt) (Å)	N_{Pt-Pt}	r(Pt–Pd) (Å)	N_{Pt-Pt}	N_{total}
Pt edge					
Dir	2.769	6.7	2.758	5.3	12.0
Imp	2.751	4.4	2.741	6.8	11.2
IE	2.738	3.4	2.735	6.1	9.5
(Metal foil)	(2.775)	(12)	–	–	12.0
Pt edge					
Dir	2.744	8.7	2.733	1.1	9.8
Imp	2.725	6.8	2.740	1.7	8.5
IE	2.738	3.8	2.743	1.3	5.1
(Metal foil)	(2.751)	(12)	–	–	12.0

N, number of atoms in the shell; r, distance from the absorber. Estimated uncertainties are r, ±0.005 Å; N, ±10%.

at 71.0 and 74.2 eV are assigned to the doublet Pt $4f_{7/2}$ and Pt $4f_{5/2}$, respectively; and that at 74.5 eV assigned to the photoemission Al 2p that corresponds to the presence of Al(III). The possible presence of a small proportion of Pt(II) cannot be totally ruled out, since this signal would be overlapped by the Al 2p signal. In the case of the catalysts prepared by ion exchange and direct incorporation, Pd is present as Pd(0) with a binding energy of 334.8 and 335.0 eV for samples PdPt-Dir and PdPt-IE, respectively. In the case of the impregnated catalyst, 80% of the Pd is as Pd(0) (335.3 eV) and 20% of Pd is oxidized to Pd(II) with a binding energy of 336.8 eV [52].

Other element-specific techniques are better adapted to the question of determining whether or not intermetallic particles have been formed. X-ray absorption spectroscopy has frequently been used to characterize bimetallic particles in this way by combining information obtained from experiments performed at each of the metal edges [53–56]. In the present work, the EXAFS signal was extracted from absorption spectra recorded at the Pd and Pt edges of samples prepared by direct incorporation, impregnation, and ion exchange. Simulation of the EXAFS obtained by Fourier filtering in the range 1.3–2.5 Å required in each case both Pd and Pt nearest neighbors, indicating the formation of intermetallic aggregates. The results of least-squares curve fitting are given in Table 3 and an example of the fits obtained at both edges in reciprocal and direct space is shown in Fig. 5 for the sample prepared by impregnation.

For bimetallic alloys, the atomic ratio and nearest neighbor environment around each element in bimetallic particles are in principle correlated through $N^{PdPt} = (X^{Pt}/X^{Pd})N^{PtPd}$

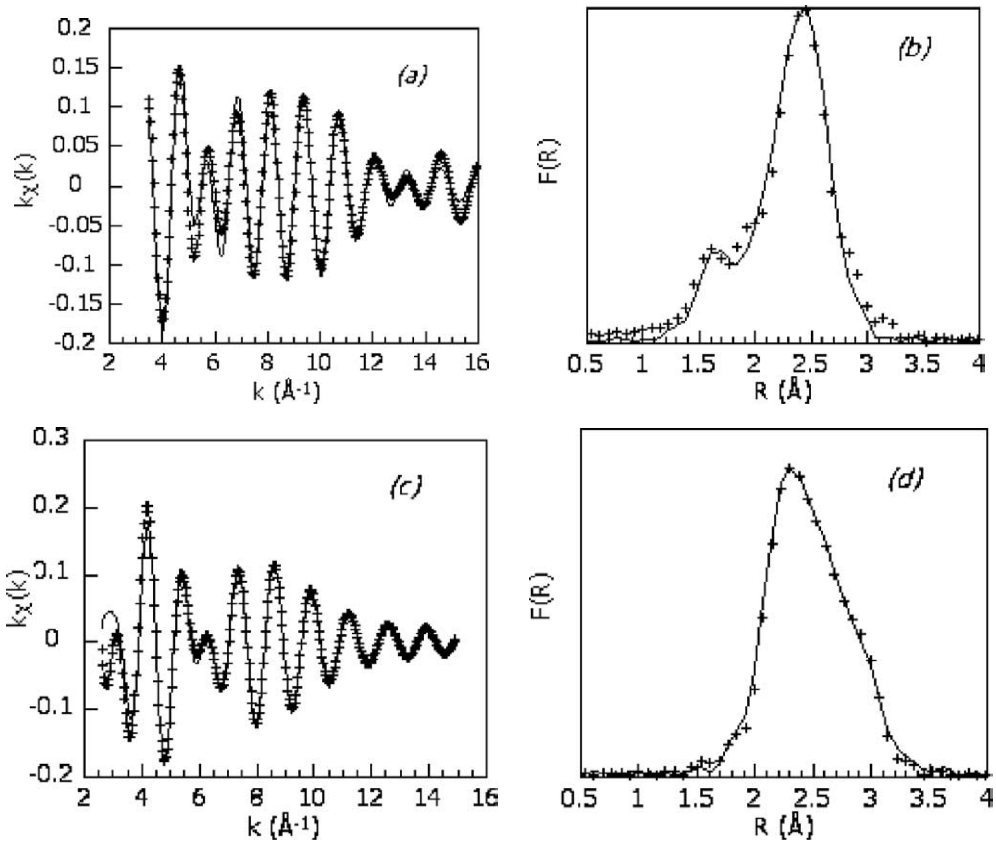

Fig. 5. Experimental (+++) and calculated (—) EXAFS spectra (a) and (c), and corresponding Fourier transforms (b) and (d) of PdPt-Imp at the Pd(a,b) and Pt(c,d) edges.

[57], where N^{PdPt} is the number of nearest Pt neighbors to Pd, N^{PtPd} the number of Pd atoms around Pt, and $X^{\mathrm{Pt}}/X^{\mathrm{Pd}}$ the atomic ratio of the two metals ($= 4$ from elemental analysis). Strong deviation from this relation would indicate segregation of the components and formation of monometallic particles. For the three catalysts, the ratio $N^{\mathrm{PtPd}}/N^{\mathrm{PdPt}}$ in materials prepared by direct incorporation, impregnation and ion exchange is 4.9, 4.0, and 4.7, respectively. While this could suggest that partial segregation occurs (monometallic Pt particles coexisting with bimetallic PdPt), these ratios are not very different from 4 when an estimated error of ±10% in the determination of the number of nearest neighbors by EXAFS is taken into account.

A second observation concerns the total number of nearest neighbors around each metal. These numbers are 12 in bulk palladium and platinum, but can be significantly lower in nanoparticles owing to the surface/volume ratio and the consequent high number of atoms that are nonsaturated coordinatively. The data of Table 3 show that the total number of nearest neighbors around each metal follows the trend in particle size identified by TEM [N_{total} (direct incorporation) $> N_{\mathrm{total}}$ (impregnation) $> N_{\mathrm{total}}$ (ion exchange)]. Segregation *within* bimetallic particles between the surface and the core is seen in EXAFS by a significantly lower coordination number around one of the two constituent elements. In the present study, strong indication that Pd is preferentially (but not exclusively) located at the surface of bimetallic particles and that Pt is preferentially (but not exclusively) situated in the core of the particle is provided by the observation that the coordination number is lower around Pd than around Pt in each catalyst, regardless of the method of incorporation of the metals. This situation seems to be characteristic of bimetallic PdPt particles [58,59], and is important in the context of catalyst thiostability [60]. This partial segregation should of course also affect the metals atomic ratio determined from the simple relationship given above. In practice, however, influence is only significant when the number of surface atoms becomes less than the number in the bulk, i.e., for particle sizes $\leqslant 2$ nm. For Pd–Pt nanoclusters obtained by laser vaporization of bulk alloys, low energy ion scattering and Monte Carlo simulations have unambiguously demonstrated surface segregation of Pd nanoparticles [61].

The interatomic distances also reflect the evolution in the particle size, with in general a reduction of bond length in smaller particles. Interatomic distances in the bulk metals are 2.751 Å for Pd–Pd and 2.775 Å for Pt–Pt. In the present case, the data of Table 3 show that the distances in the supported metal particles are always shorter than those of the bulk metal foils. A further parameter to be considered is the possibility of partial oxidation of the metal particles, as well as interaction with the surface of the support oxide, since strong interaction between the metal ions and the support

oxide could reduce accessibility of the metal, and/or limit the extent of reduction at the particle surface. Only in the case of the catalyst prepared by impregnation could a shell of two oxygen neighbors at a distance of 2.01 Å from Pd could be identified from EXAFS, a result in agreement with those from XPS.

The preceding characterization using a range of techniques shows that metal particles in the above catalyst materials prepared using the same support by ion exchange, impregnation and direct incorporation have distinct properties. Of the three samples, those prepared by ion exchange and impregnation have higher metal dispersion and available metal surface area than that prepared by direct incorporation, while the BET surface area is smaller for the ion-exchanged catalyst than the impregnated material. These characteristics, in conjunction with our conclusions from XPS and EXAFS spectroscopies, led us to select the material prepared by impregnation for evaluation as hydrogenation/ring-opening catalyst.

3.2. Hydrogenation/ring opening of naphthalene

3.2.1. Catalytic activity at atmospheric pressure

Preliminary tests to assess hydrogenation and hydrogenolysis/ring-opening activity of the PdPt-Imp material were carried out at atmospheric pressure. The reaction is thermodynamically limited at this pressure, and the conversion decreases rapidly as the temperature is increased. The conversion and selectivity to decalins (*cis*- and *trans*-decahydronaphthalene), tetralin (1,2,3,4-tetrahydronaphthalene), hydrogenolysis/ring-opening products (e.g., cyclohexane, toluene, xylene, alkylbenzenes, decadiene), and light (C_1–C_4) fractions are shown in Table 4. At 200 °C, conversion of naphthalene by the material is 98.9% while at 300 °C, the conversion is significantly lower (7.9%). Further, at 200 °C the material gives pronounced selectivity to decalin (96.1%), as previously observed also over monometallic Pd or Pt catalysts at this temperature [36,62]. At 300 °C, tetralin is formed mainly (96.2%), but there is also an increase of molecules resulting from hydrogenolysis/ring-opening reactions: alkylbenzenes and decadiene etc., representing 4% of the reaction products.

In the presence of benzo(*b*)thiophene at 200 °C the selectivity to decalin changes with time (Fig. 6a). Over 17 pulses of benzo(*b*)thiophene, the conversion of naphthalene decreased from 99 to 93%, but the selectivity switched from decalin to tetralin after 11 pulses. For comparison, this test was also carried out using a monometallic Pt (2 wt%) catalyst prepared by impregnation in an identical fashion and with the same SiAl20 support. This catalyst had a metal dispersion of 34%. In this case, conversion dropped to 72% after only 6 injections of benzo(*b*)thiophene (Fig. 6b), clearly indicating improved sulfur tolerance for the bimetallic Pd/Pt catalyst. It is well known that activity can be modified by poisoning without affecting the selectivity [63]. In the case of multifunctional catalysts, having active sites of different nature (for example, acid and metal) whose role is to simultaneously promote different steps or chemical trans-

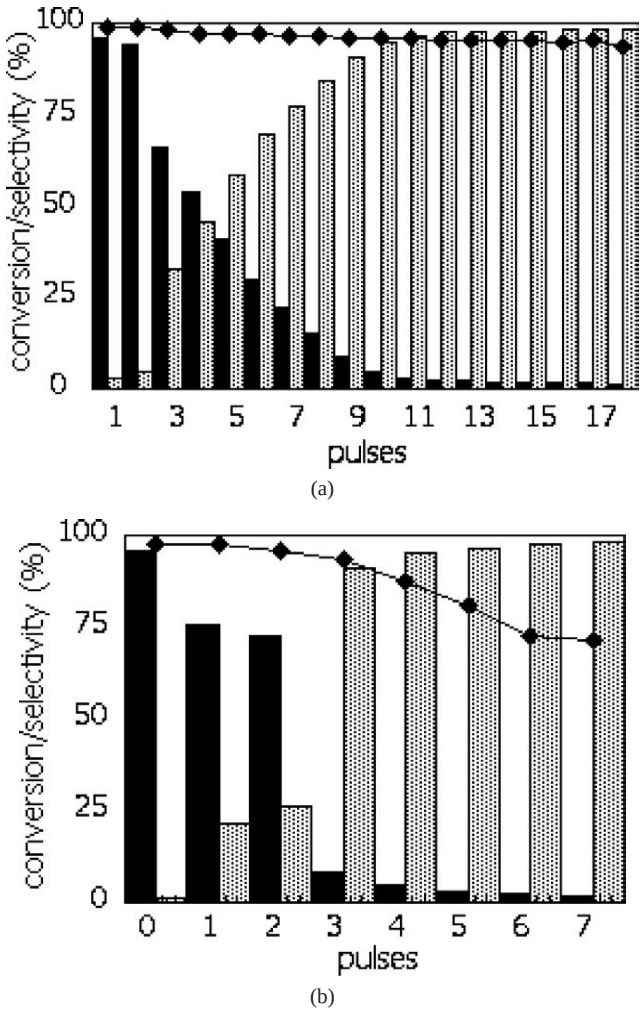

Fig. 6. Conversion of napththalene in the presence of benzo(*b*)thiophene at 200 °C and atmospheric pressure. PdPt-Imp (a) and Pt-containing catalysts (b). Production of ■: decalin (%); ▩: tetralin (%); ◆: naphthalene conversion (%).

Table 4
Conversion of naphthalene and product distribution at 200 and 300 °C and atmospheric pressure given by PdPt-Imp

Temperature (°C)	Conversion (%)	Selectivity (%)[a]							Yield
		Decalin	Tetralin	Cyclohexane	C_1–C_4	Toluene, *o*-xylene	Alkyl-benzenes	Decadiene	
200	98.9	96.1	2.8	–	–	–	1.1	–	1.09
300	7.9	–	96.2	–	–	–	1.3	2.5	0.30

[a] Yield in high molecular weight hydrogenolysis/ring-opening products (sum of alkylbenzenes and decadiene × conversion).

formations, the deactivation of one type of site can lead to a modification of selectivity. In the present case, the PdPt-Imp catalyst, which gave mainly decalin in the sulfur-free feed, produces progressively partial hydrogenation of naphthalene to tetralin in the presence of benzo(*b*)thiophene. This increasing selectivity to tetralin caused by sulfur poisoning is accompanied by a slight decrease in conversion due either to a modification of the active sites and/or the formation of sulfides.

It may be concluded that the monometallic platinum catalyst is not sulfur resistant whereas the Pd/Pt catalyst has a much higher sulfur tolerance. This result confirms the conclusions in the literature indicating that the formation of a noble metal alloy, particularly with Pd, is beneficial for sulfur resistance [14]. This sulfur resistance can also be related to the method of metal incorporation, which affects the nature and the structure of the metal particles formed: intermetallic particles or segregated metallic phases, the degree of dispersion, and the nature of the interaction with the support [21].

3.2.2. Catalytic activity at 6.0 MPa

The activity of the PdPt-Imp for naphthalene hydrogenation as a function of temperature at 6.0 MPa is shown in Fig. 7 where it is compared with that of the reference catalyst. The activity is generally comparable to that of the reference catalyst with formation of low quantities of tetralin, and a rather high negative carbon balance due to the formation of low molecular weight (LMW) products. Above 260 °C, the catalyst shows a good activity in hydrogenation, with 99.6% of naphthalene conversion and formation of 41.6% of decalins. In the temperature range 260–340 °C, a significant quantity of high molecular weight (HMW) products is formed; however, beyond 300 °C, cracking reactions to LMW products predominate. Addition of DBT to the feed (100 to 3000 ppm) leads to a progressive decrease in hydrogenation and hydrogenolysis/ring-opening reactions, with formation of an increasing quantity of tetralin and LMW cracking products.

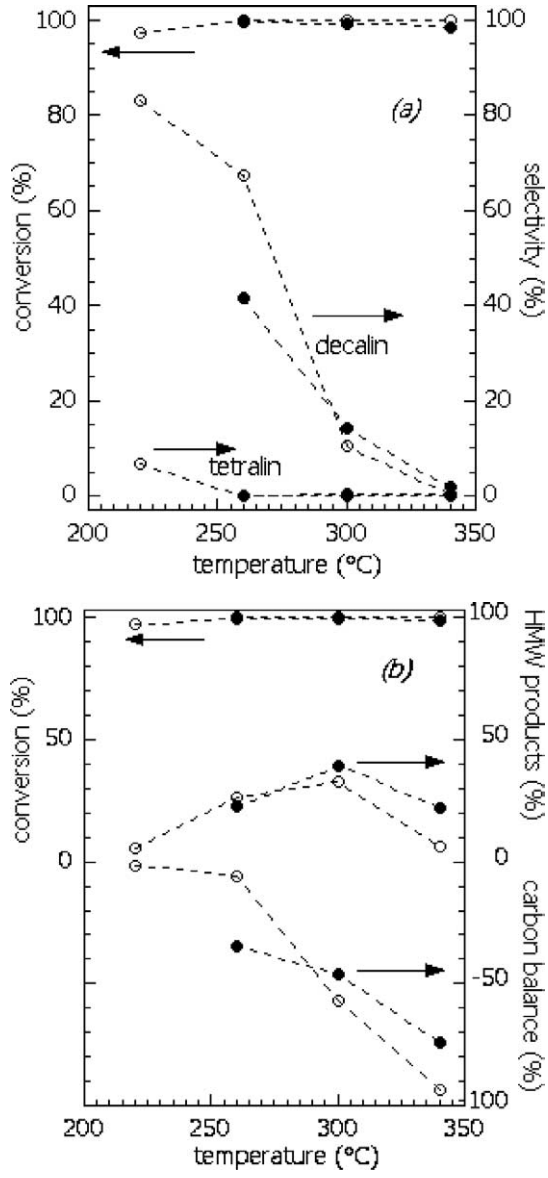

Fig. 7. Activity in naphthalene hydrogenation [conversion (%), selectivity in decalin/tetralin (%) and high molecular weight products (HMW), carbon balance (%)] of PdPt-Imp (●) and the reference catalyst (○).

3.3. Catalytic evaluation on an industrial diesel

The behavior of the PdPt-Imp catalyst on a hydrotreated LCO/SR diesel feedstock (Table 5) under industrial conditions was evaluated in terms of aromatic saturation, cetane number improvement, and product distribution of the $< 180°$ cracking products fraction, and its behavior compared to that of the zeolite-type reference catalyst [12].

Between 270 and 300 °C, saturation of aromatics in the feed increases from 40 to 90% (Fig. 8). Over the same temperature range, the reference catalyst gives only 55% aromatic saturation, higher temperatures being required to further increase hydrogenation (to 80% at 315 °C). Since saturation of 80% of the aromatics is achieved by PdPt-Imp at only 285 °C, there is therefore a significant temperature advantage. Aromatic saturation and ring opening lead to an increase in the cetane number, which was determined for the products at the different temperatures according to ATSM-D-4737. The results are represented in Fig. 9 as the cetane number increase, ΔCN. Using the PdPt-imp catalyst, cetane number is increased by 5 points at 270 °C and by 7.5 points at 300 °C, representing an improvement of 22% compared with that of the feed (36.6). In contrast, at 300 °C, the reference catalyst produces a more modest improvement of 5 points, an improvement of 13.6% compared with that of the feed. In addition to the objective of aromatics saturation and cetane number improvement, it is essential from an economics point of view that loss of yield by cracking to low-value light gases be as low as possible. Fig. 10 shows that although the formation of nonselective cracking products increases with temperature, at 300 °C the production

Table 5
Characteristics of LCO/SR feedstocks and following two-stage upgrading by hydrotreating (HT) and hydrogenation/ring opening (RO)

Feed number	1	3	HT1	HT3	RO
Composition	LCO/SR (85:15 wt%)	LCO/SR (85:15 wt%)	Hydrotreated 1	Hydrotreated 3	
Operating conditions of hydrotreating			6.0 MPa, 1 h^{-1}, 390 °C, 400 N cm^3 H_2/cm^3 feed	6.0 MPa, 1 h^{-1}, 360 °C, 400 N cm^3 H_2/cm^3 feed	
Sulfur (ppm)	19,400	19,000	52	32	< 1
Nitrogen (ppm)	1194	1400	138	10	< 1
Aromatics (*HPLC*) (*IP-391/95*) (*wt%*)					
Monoaromatics	24.21	20.67	49.3	44.76	< 10
Diaromatics		32.84	12.95	7.33	
Triaromatics		15.84	4.58	2.93	
Polyaromatics (Di+)	38.96	48.68	17.53	10.26	< 3
Total	63.17	69.35	66.83	55.02	
Density, 15/4 °C[a] (g/cm^3)	0.9313	0.9488	0.8926	0.8914	0.8400
Viscosity, 40 °C[b]	3.169	3.998	2.700	3.176	
Distillation[c] (*vol%*)					
180 °C−	0	0	0	0	9
180–360 °C	90	89	93	93	89
360 °C+	10	11	7	7	2
T95%	379	386	376	368.5	354
IBP[d]	197	222	188	200.2	104
EBP[e]	390	394	386	383.5	375
Cetane index[f]	28.9	27.2	35.3	36.6	45–46

[a] Density in the range 15–4 °C, according to ASTM-D-4052 (1996).
[b] According to ASTM-D-445.
[c] According to ASTM-D-86.
[d] Initial boiling point.
[e] End boiling point.
[f] According to ASTM-D-4737.

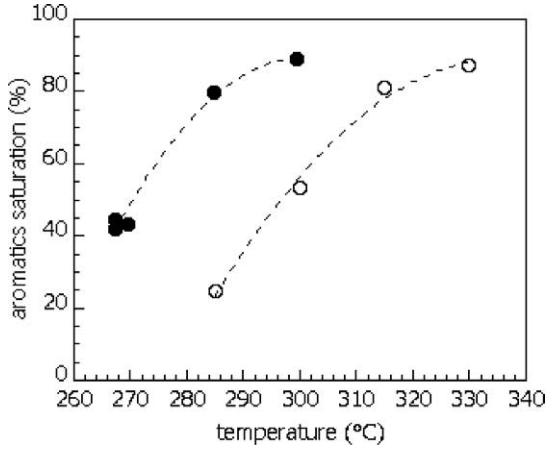

Fig. 8. Aromatics saturation given by the PdPt-Imp catalyst compared with the reference catalyst. ●, PdPt-Imp on feed HT3; ○, reference on feed HT1 (see Table 5).

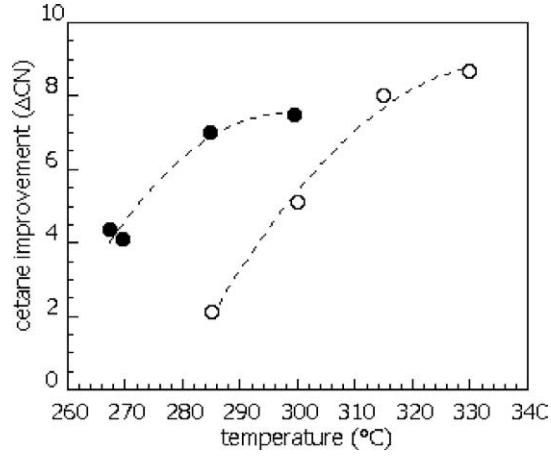

Fig. 9. Cetane number improvement with the PdPt-Imp catalyst; comparison with the reference catalyst. ●, PdPt-Imp on feed HT3; ○, reference on feed HT1 (see Table 5).

of compounds with boiling point < 180 °C is < 1% while for an equivalent cetane number improvement by the reference catalyst, losses are ca. 6%. Figs. 8–10 also show that the maximum of activity of the reference catalyst is reached at a higher temperature: at 330 °C, 90% aromatic saturation is observed and a cetane number increase of 8.5 points, but the nonselective cracking is higher, reaching 10%. Fujikawa et al. [21,64] have investigated nonzeolite supported bimetallic catalysts on hydrotreated LCO/SRLGO feed (less than 500 wt ppm sulfur). PdPt/SiO_2–Al_2O_3 was the most active catalyst with the coexistence of Pd with Pt increasing the catalytic activity, this activity depending on synthesis conditions and Pd/Pt ratio [21]. The use of Pt(0.5%)–Pd(1%)/SiO_2/Al_2O_3 on such feed led to products of good quality, with increased cetane index and decreased sulfur content (50 wt ppm sulfur achieved) [64]. In the present

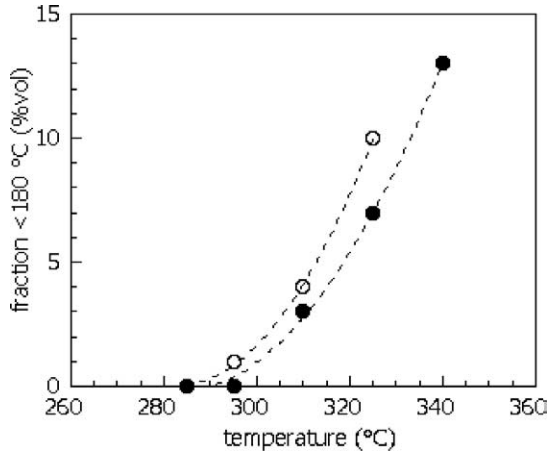

Fig. 10. < 180 °C fraction obtained with the PdPt-Imp catalyst and the reference catalyst. ●, PdPt-Imp on feed HT3; ○, reference on feed HT1 (see Table 5).

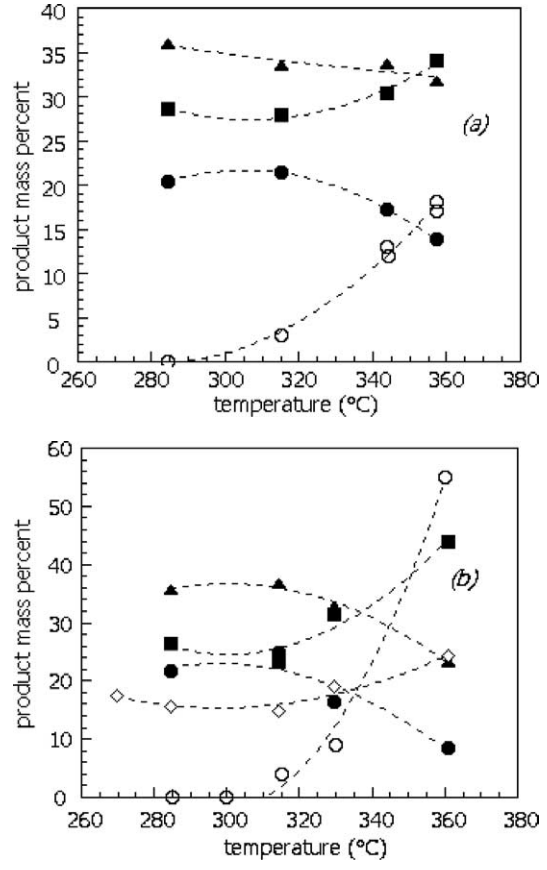

Fig. 11. Influence of temperature on hydrogenolysis/ring-opening and cracking reactions for the PdPt-Imp catalyst (a) and the reference catalyst (b). ■, 1-ring; ▲, 2-ring; ●, 3-ring; ○, cracking (< 180 °C, vol%); ◇, noncyclic paraffins.

case, mass spectroscopic analysis of liquid samples obtained in the activity tests at different temperatures was carried out to follow changes in the amount of cyclic components with 1, 2, and 3+ rings. The results, shown in Fig 11a, show the proportion of 2-ring compounds to remain essentially constant, while that of 1-ring compounds increases above ca. 310 °C at the expense of the 3+ ring component. This hydrogenolysis/ring-opening activity takes place at the same temperature as the onset of nonselective cracking. The behavior of the reference catalyst (Fig. 11b) shows a slightly different temperature dependence, 1-ring compounds increasing as the proportion of both 2− and 3+ rings decreases above ca. 315 °C. Again, nonselective cracking reactions take place concomitantly.

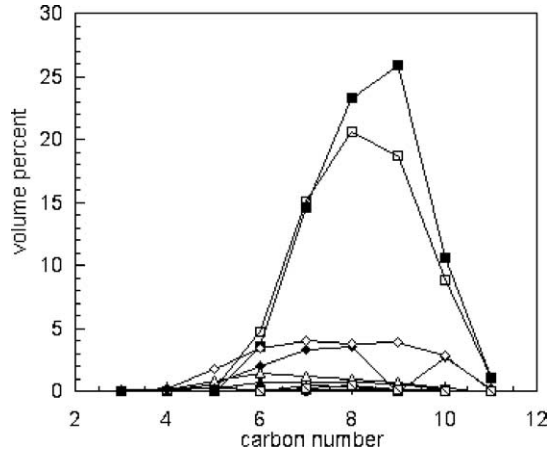

Fig. 12. Identification of nonselective cracking products obtained with PdPt-Imp, at 300 and 325 °C. At 300 °C, ■, naphthenes; ◆, *i*-paraffins; ▲, *n*-paraffins; ▼, cyclo-olefins; ●, *i*-olefins; ×, *n*-olefins; ◫, aromatics. At 325 °C, □, naphthenes; ◇, *i*-paraffins; △, *n*-paraffins; ▽, cyclo-olefins; ○, *i*-olefins; +, *n*-olefins; ◪, aromatics.

The identification of nonselective cracking products is a further important step which can indicate if the formed products can be used or not in other refinery processes. From Fig. 12, it may be seen that in the case of < 180 °C range products formed in reactions catalyzed by the PdPt-Imp catalyst, C_7–C_{10} naphthenes clearly predominate, and represent 73 and 61% of the total volume at 300 and 325 °C, respectively. Branched C_7–C_{10} alkanes account for a further 9 and 15 vol%, respectively. Both these naphthene and *iso*-alkane fractions can be used in other reforming processes. The results of this analysis indicate that although nonselective cracking reactions represent a loss of the initial LCO feed, they give either directly useful products (kerosene, heavy naphtha) or compounds useful for other reactions (reforming). Finally, the nature of the product spectrum is compatible with naphthene formation either via hydrogenation of both rings of diaromatic alkylbenzenes, followed by hydrogenolysis/ring opening and cracking, or with hydrogenation of a single ring followed only by hydrogenolysis plus cracking, followed by a further hydrogenation step.

4. Conclusion

The objective of this research was to prepare catalysts combining the hydrogenation–hydrogenolysis/ring-opening activity of one metal with thioresistance of the other, in

nonsegregated particles. While the direct incorporation of salts, metallic alkoxides, or propanedioanates is a simple "one-pot" method for the preparation of bimetallic catalysts adapted to the surfactant containing reaction medium, impregnation or ion exchange on a support gives more satisfactory results in terms of the final metal particle size. Pores in the preformed matrix restrain the growth of metal particles, whereas in the synthesis gel, both condensation of the aluminosilicate matrix and metal oxide particle growth take place at the same time.

The association of a range of different techniques including adsorption from the gas phase and element-specific spectroscopies (such as XPS and EXAFS) provide converging results, indicating the existence of intermetallic particles, the latter method also enabling us to conclude that palladium is preferentially located on the particle surface. The higher catalytic activity at lower temperatures of the impregnated catalyst compared with that of a reference state-of-the-art zeolite-based catalyst under industrial conditions on a hydrotreated light cycle oil is a promising result, and the further improvement of this material, in particular by increase of its sulfur tolerance and selective hydrogenolysis/ring-opening capacity, will be the objective of our future studies.

Acknowledgment

Financial support under the European Commission's Brite-EuRam programme, contract number BRPR-CT97-0560 is acknowledged with thanks.

References

[1] A. Arcoya, A. Cortes, J.L.G. Fierro, X.L. Seoane, Stud. Surf. Sci. Catal. 68 (1991) 557.
[2] J. Barbier, E. Lamy-Pitara, P. Macelot, J.P. Boitiaux, J. Cosyns, F. Verna, Adv. Catal. 37 (1990) 279.
[3] J.P. Peries, A. Billon, A. Hennico, S. Kressmann, NPRA 89th Annual Meeting, San Antonio, TX, 1991.
[4] J.P. Lucien, G.G.V.D. Berg, H.M.J.H.V. Hooijdonk, M. Gjers, G.L.B. Thielsman, Catalyst Hydroprocessing of Petroleum and Distillates, Decker, New York, 1994, p. 291.
[5] J.P. Lucien, G.L.B. Thielemans, Eur. patent 0,512,652,A1 (1992), to Shell Internationale Research Maatschappij B.V.
[6] A.J. Suckanek, Oil Gas J. 7 (May) (1990) 109.
[7] R.R. Lawrence, JPI Conference, Tokyo, Japan 2–3 October, 1996.
[8] B.H. Cooper, P. Søgaard-Andersen, P.N. Hannerup, in: AIChE Spring National Meeting, Houston, TX, 1993.
[9] B.H. Cooper, A. Stanislaus, P.N. Hannerup, ACS Div. Fuel Chem. 37 (1992) 41.
[10] P. Søgaard-Andersen, B.H. Cooper, P.N. Hannerup, NPRA Annual Meeting, New Orleans, LA, 1992.
[11] S.G. Kukes, F.T. Clark, D. Hopkins, US patent 5,147,526 (1992), to Amoco Corporation.
[12] S.G. Kukes, F.T. Clark, D. Hopkins, WO patent 94/19429 (1994), to Amoco Corporation.
[13] S.G. Kukes, F.T. Clark, D. Hopkins, L.M. Green, US patent 5,151,172 (1992), to Amoco Corporation.
[14] H. Yasuda, Y. Yoshimura, Catal. Lett. 46 (1997) 43.
[15] H. Yasuda, T. Sato, Y. Yoshimura, Catal. Today 50 (1999) 63.
[16] L. LeBihan, Y. Yoshimura, Fuel 81 (2002) 491.
[17] B. Pawelec, R. Mariscal, R.M. Navarro, S.v. Bokhorst, S. Rojas, J.L.G. Fierro, Appl. Catal. A 225 (2002) 223.
[18] S. Murcia-Mascarós, B. Pawelec, J.L.G. Fierro, Catal. Commun. 3 (2002) 305.
[19] J.L. Rousset, L. Stievano, F.J.C.S. Aires, C. Geantet, A.J. Renouprez, M. Pellarin, J. Catal. 202 (2001) 163.
[20] J.E. Naber, W.H.J. Stork, in: Proceedings of First Japan-EC Joint Workshop on the Frontiers of Catalytic Science and Technology for Alternative Energy and Global Environmental Protection, Tokyo, Japan, 1991.
[21] T. Fujikawa, K. Idei, T. Ebihara, H. Mizuguchi, K. Usui, Appl. Catal. A 192 (2000) 253.
[22] M. Vaarkamp, B.H. Reesink, P.H. Berben, WO patent 98/35754 (1998), to Engelhard.
[23] R. Navarro, B. Pawelec, J.M. Trejo, R. Mariscal, J.L.G. Fierro, J. Catal. 189 (2000) 184.
[24] T. Fujikawa, K. Idei, K. Usui, Sekiyu Gakkaishi 42 (1999) 271.
[25] H. Yasuda, T. Kameoka, T. Sato, N. Kijima, Y. Yoshimura, Appl. Catal. A 185 (1999) L199.
[26] V.L. Barrio, P.L. Arias, J.F. Cambra, M.B. Güemez, B. Pawelec, J.L.G. Fierro, Fuel 82 (2003) 501.
[27] E. Rodríguez-Castellón, J. Mérida-Robles, L. Díaz, P. Maireles-Torres, D.J. Jones, J. Rozière, A. Jiménez-López, Appl. Catal. A 260 (2004) 9.
[28] A. Corma, V. González-Alfaro, A.V. Orchillés, J. Catal. 200 (2001) 34.
[29] S. Albertazzi, N. Donzel, M. Jacquin, D.J. Jones, M. Morisi, J. Rozière, A. Vaccari, Catal. Lett. 96 (2004) 157.
[30] A. Corma, V. González-Alfaro, A.V. Orchillés, A. Martínez, V. Martínez-Soria, J. Catal. 153 (1995) 25.
[31] A. Corma, A. Martínez, V. Martínez-Soria, J. Catal. 169 (1997) 480.
[32] A. Corma, A. Martínez, A. Martínez-Soria, J. Catal. 200 (2001) 259.
[33] J. Rozière, M. Brandhorst, R. Dutartre, M. Jacquin, D.J. Jones, P. Vitse, J. Zajac, J. Mater. Chem. 11 (2001) 3264.
[34] A. Corma, V. Fornes, M.T. Navarro, J. Perez-Parinete, J. Catal. 148 (1994) 569.
[35] M.J. Meziani, J. Zajac, J.M. Douillard, D.J. Jones, S. Partyka, J. Rozière, J. Colloid Interface Sci. 233 (2001) 219.
[36] M. Jacquin, D.J. Jones, J. Rozière, S. Albertazzi, A. Vaccari, M. Lenarda, L. Storaro, R. Ganzerla, Appl. Catal. A 251 (2003) 131.
[37] S. Rojas, P. Terreros, M.A. Peña, M. Ojeda, J.L.G. Fierro, A. Otero, F. Carrillo, J. Mol. Catal. A: Chem. 206 (2003) 299.
[38] R.S. Mulukutla, K. Asakura, S. Namba, Y. Iwasawa, Chem. Commun. (1998) 1425.
[39] S. Albertazzi, C. Gobbi, R. Ganzerla, M. Lenarda, M. Mandreoli, E. Salatelli, P. Savini, L. Storaro, A. Vaccari, J. Mol. Catal. A: Chem. 200 (2003) 261.
[40] T. Sun, J.Y. Ying, Nature 389 (1997) 704.
[41] G. Fryxel, J. Liu, Surf. Sci. Ser. 90 (2000) 665.
[42] S. Brunauer, P.H. Emmet, F. Teller, J. Am. Chem. Soc. 16 (1938) 309.
[43] A. Michalowicz, Logiciels pour la Chimie, Société Française de Chimie, Paris, 1991, p. 102.
[44] J.J. Rehr, C.H. Booth, F. Bridges, S.I. Zabinsky, Phys. Rev. B 49 (1994) 12,347.
[45] S.D. Lin, C. Song, Catal. Today 31 (1996) 93.
[46] C. Petitto, G. Giordano, F. Fajula, C. Moreau, Catal. Commun. 3 (2002) 15.
[47] T. Rades, M. Polisset-Thfoin, J. Fraissard, Top. Catal. 11/12 (2000) 283.
[48] P.L. Hansen, A.M. Molenbroek, A.V. Ruban, J. Phys. Chem. B 101 (1997) 1861.
[49] U. Junges, S. Disser, G. Schid, F. Schüth, Stud. Surf. Sci. Catal. (1998) 391.
[50] J.L. Rousset, F.J.C.S. Aires, F. Bornette, M. Cattenot, M. Pellarin, L. Stievano, A.J. Renouprez, Stud. Surf. Sci. Catal. 117 (2000) 391.

[51] P. Gallezot, C. Leclercq, in: B. Imelik, J.C. Vedrine (Eds.), Catalyst Characterization, Plenum, New York, 1994, p. 537.
[52] J.F. Moulder, W.F. Stickle, P.E. Sobol, K.D. Bomben, Standard Spectra for Identification and Interpretation of XPS data, Perkin-Elmer, Eden Prairie, MN, 1992.
[53] L.E. Aleandri, B. Bogdanovic, C. Dürr, S.C. Huckett, D.J. Jones, U. Kolb, M. Lagarden, J. Rozière, U. Wilczok, Chem. Eur. 3 (1997) 1710.
[54] N. Toshima, M. Harada, T. Yonezawa, K. Kushihashi, K. Asakura, J. Phys. Chem. 95 (1991) 7448.
[55] M. Harada, K. Asakura, Y. Ueki, N. Toshima, J. Phys. 97 (1993) 10,742.
[56] U. Kolb, S.A. Quaiser, M. Winter, M.T. Reetz, Chem. Mater. 8 (1996) 1889.
[57] G.H. Via, K.F.J. Drake, G. Meitzner, F.W. Lytle, J.H. Sinfelt, Catal. Lett. 5 (1990) 25.
[58] T. Fujikawa, K. Tsuji, H. Mizuguchi, H. Godo, K. Idei, K. Usui, Catal. Lett. 63 (1999) 27.
[59] E. Guillon, J. Lynch, D. Uzio, B. Didillon, Catal. Today 65 (2001) 201.
[60] N. Matsubayashi, H. Yasuda, M. Imamura, Y. Yoshimura, Catal. Today 45 (1998) 375.
[61] J.L. Rousset, A.J. Renouprez, A.M. Cadrot, Phys. Rev. B 58 (1998) 2150.
[62] A.D. Schmitz, G. Bowers, C. Song, Catal. Today 31 (1996) 45.
[63] P. Fortazzi, L. Lietti, Catal. Today 52 (1999) 165.
[64] T. Fujikawa, K. Idei, K. Ohki, H. Mizuguchi, K. Usui, Appl. Catal. A 205 (2001) 71.